Accelerated aging modulates the toxicological properties of the diazo tattoo pigment PO13

Lise Aubry, Marianne Vitipon, Aurélie Hirschler, Hélène Diemer, Thierry Rabilloud, Christine Carapito, Thierry Douki

scientific reports

Check for updates

OPEN

Accelerated aging modulates the toxicological properties of the diazo tattoo pigment PO13

Lise Aubry[1], Marianne Vitipon[2], Aurélie Hirschler[3,4], Hélène Diemer[3,4], Thierry Rabilloud[2], Christine Carapito[3,4] & Thierry Douki[1]✉

Pigment particles used in tattooing may exert long terms effect by releasing diffusible degradation products. In the present work, aqueous suspensions of the organic orange diazo pigment PO13 were aged by exposure to simulated sunlight at 40 °C. The morphology and the surface charge of PO13 particles were barely modified upon aging, but primary particles were released by de-agglomeration. Soluble photoproducts were detected in the liquid fractions. One of this photoproduct (DCBP) was produced in large amount in suspension in isopropanol and purified. The toxicological profiles of aged suspensions, their soluble fractions and DCBP were then determined on the keratinocyte cell line HaCaT. Impact of suspensions of PO13 on viability was hardly affected by aging. In contrast, the soluble fractions were more toxic after photo-aging. Suspensions and filtrates induced neither release of reactive oxygen species nor formation of DNA strand breaks. The samples exhibited only limited effects on the proteome of HaCaT cells. Conversely, DCBP was cytotoxic and induced the production of ROS, but was not genotoxic. DCBP was found to activate CYP450 monooxygenases known to be involved in the metabolism of xenobiotics. Altogether, our results show that aging of PO13 leads to the release of toxic soluble compounds.

Keywords Tattoo, Skin toxicity, Photodegradation, Photoproduct, Proteomics

Tattooing is a growing trend around the word, especially in industrialized countries. From one country to another, the prevalence is estimated to range from 11.7 to 31.5% in the overall population[1]. Tattooing consists in the injection of inks containing pigments into the dermis, just below the epidermaldermal junction. The amount of pigment injected in the skin has been estimated to be between 0.60 and 9.42 mg $cm^{[-2}$ [2]. Pigments are insoluble particles that provide the persistent tints to the tattoo. The long lifetime of tattoo is explained by the internalization of pigments by dermal macrophages. This process, which lasts overtime by a release-recapture cycle at each macrophage death, allows the pigments to be permanently maintained in the dermis[3]. Pigments may be black, white or colored depending on their chemical nature. Many mineral pigments based on heavy metals (e.g. cadmium) have been used in the past and are now banned because of toxicity issues. Colored pigments are now mostly organic compounds, such as polycyclic and azo pigments. The recent European Union legislation about tattoo pigments has banned, based on toxicological considerations, the sale of tattoo inks containing azo pigments and some organometallic ones like Pigment blue 15:3, a copper phthalocyanine[4]. Yet, their use remains an issue[5;6] because of the persistence of tattoos made before the enforcement of the regulation and because of the use of unapproved inks in some tattooing studios.

Numerous studies have been devoted to the immediate deleterious effects of tattooing such as inflammation[7,8]. In contrast, only few information are available on the longterm or permanent toxicity of organic pigments for the skin. This is yet mandatory for products aimed at remaining for years and decades in tissues. Several aspects have to be considered. Possible adverse reactions include allergy or phototoxicity. Indeed, clinical cases of allergic reaction in tattoos containing organic pigments have been reported several times. They can occur from immediately up to 7 years after tattooing, and some of these cutaneous reactions follow UV exposure[9,10]. In a study on tattooed sunbathers, Hutton et al.[11]noticed that 20% of them had suffered of sun-related symptoms in their tattooed skin. Other consequences of sun exposure of tattoos is the photosensitizing properties of some of their impurities, like benzo[g, h,i]perylene in black pigments[12]. Another important consequence could also be

[1]Univ. Grenoble Alpes, CEA, CNRS, Grenoble INP, SyMMES, Grenoble F-38000, SyMMES, France. [2]Chemistry and Biology of Metals, Univ. Grenoble Alpes, CNRS UMR5249, CEA, IRIG-LCBM, Grenoble F-38054, France. [3]Laboratoire de Spectrométrie de Masse BioOrganique (LSMBO), Université de Strasbourg, CNRS, IPHC UMR 7178, Strasbourg F-67000, France. [4]Infrastructure Nationale de Protéomique ProFI – FR2048, Strasbourg 67087, France. ✉email: thierry.douki@cea.fr

cutaneous carcinogenesis. Today, there is no proven link between skin cancer and tattooed skin. However, some clinical cases of malignant melanoma and keratinocytic carcinoma, including squamous cell carcinoma (SCC) and basal cell carcinoma (BCC), in tattooed people have been reported, although some authors consider them as coincidental regarding the weak occurrence of these cases in tattooed population[13]. Nevertheless, Leijs et al.[14] have published a case series of six tattooed patients with skin malignancies. They noticed that the patients were younger compared to typical clinical cases reported in epidemiological data.

The biochemical and molecular bases of potential toxicological effects of tattoo pigments are also poorly investigated. This is yet a major issue since pigments are internalized in macrophages and are only shortly free in the dermis during the macrophagic release-recapture process. One possible toxicological pathway could be the degradation of pristine pigments into smaller size particles or low molecular weight soluble compounds that could freely diffuse from the dermis and reach other sites in the body, such as the epidermis where keratinocytes are the predominant cell population. Such a process could be biologically relevant as some studies indicate that azo pigments could be cleaved by light into potential hazardous compounds[15–18]. Moreover, Sepehri et al.[19]have shown blood distribution of pigments in tattooed mice by demonstrating particles deposition in the liver, more precisely in the Kupffer cells. Experiments involving phthalocyanine pigments also led to the observation of release of toxic degradation products[20,21].

One possible degradation mechanism could be driven by the oxidative and acidic conditions encountered in the phagolysosomal environment of dermal macrophages. This has been observed for some inorganic pigments, for example by Devcic et al.[22]who highlighted their degradation by cultured macrophages. Another mechanism could be the combined action of longterm chemical aging and photochemical processes triggered by solar visible and ultraviolet radiations. Indeed, light could alter azo pigments such as Pigment yellow 74 (PY74) and Pigment red 22 (PR22). Two studies have demonstrated that these pigments, when dissolved in organic solvents, could be degraded by simulated or natural solar light exposure[15,18]. More interestingly, Engel et al.[16]observed a significant decomposition of PR22 in tattooed SKH-1 mice after a 32 day exposure to simulated solar radiation. Evidence were also provided for the sunlight-induced decomposition of Acid Red 87[23].

In the present work, we explored the toxicological consequences of photoaging of the organic diazo pigment Pigment orange 13 (PO13, C.I. 21110, CAS. No. 3520–72 – 7). A study carried out by Hauri and Hohl[17]had previously revealed photodegradation of an ink containing PO13 after exposure to visible light for 7 days. Otherwise, no study was carried out to assay toxicity of PO13 after aging by solar light in a keratinocyte or any human cell models[24]. Our first objective was thus to characterize the potential modifications of physicochemical properties of PO13 upon exposure to simulated sunlight. Then, the second objective aimed at investigating differences in the toxicological profile of PO13 after photo-aging in a well-characterized keratinocytes model, the HaCaT cell line. The third part focused on the characterization and the toxicological assessment in HaCaT cells of the major PO13 photoproduct. In the two latter parts, in vitro toxicological assays were combined with mass spectrometry-based differential proteomic analysis to gather wide information on the cellular responses.

Methods

Chemicals

Pigment orange 13 was purchased from Santa Cruz Biotechnology (Dallas, USA). The purity of the batch used was 91.2% with 1.1% moisture. The water used for the preparation of suspensions and of HPLC solvents was purified in a MilliQ direct 8 system (Millipore). Acetonitrile (Carlo Erba) used for HPLCmass spectrometry analyses was of LCMS grade. Ammonium formate and formic acid (Aldrich) used for the HPLC buffers were of the highest purity available.

Photoaging of PO13 suspensions

Suspensions of PO13 at 10 mg mL^{-1} were prepared in water. Pigment particles were dispersed by sonication for 15 min and an amplitude of 60% in a cuphorn instrument (BioBlock Scientific, France). The temperature was kept at 4 °C by a thermostated water circulation. Then, PO13 suspensions were transferred, together with a 0.7 cm magnetic bar, into 1 × 1 × 3.5 cm spectrophotometer quartz cuvettes sealed with a screw cap. The samples were placed, under constant magnetic stirring, in a QSUN XE-1 Xenon Test Chamber (LX-5080TM, Qlab, USA) for 96 h. The photo-aging conditions followed the ISO 4892-2guidelines for materials testing[25]. The temperature within the sample was set at 40 °C. Simulated sunlight (both ultraviolet and the visible wavelengths) was applied at an intensity corresponding to an equatorial sun (1.44 W m^{-2} nm^{-1} measured at 420 nm). Two control samples were also prepared (i) a PO13 suspension incubated under agitation for 96 h at 40 °C in the dark, and (ii) a pristine suspension kept in the dark at 4 °C. Aliquot fractions (500 µL) of the suspensions were centrifuged (8000xg, 10 min) in filtering tubes bearing a 0.2 µm nylon membrane (VWR). Another aliquot fraction of suspension (100 µL) was centrifuged (8000xg, 10 min) and the liquid fraction was discarded. Hundred µL of octanol was added. The sample was vortexed and transferred to a 0.2 µm filtering tube. After centrifugation, the filtrate was transferred to HPLC vials.

Physicochemical characterization

Measurements of zeta potential and hydrodynamic diameter of PO13 particles were performed on a Litesizer 500 particle analyzer (Anton Paar GmbH, Graz, Austria) using electrophoretic and dynamic light scattering, respectively. For the former technique, samples were diluted in 1/1000 PBS. For DLS, samples were analyzed at different dilutions in water in order to perform reliable measurements. The UV-visible absorption spectra were recorded on a Cary 60 UV-Vis spectrophotometer (Agilent Technologies, Santa Clara, CA). Samples were solubilized in DMF.

High performance liquid chromatography associated with electrospray tandem mass spectrometry (HPLC-MS/MS)

Filtrate of the PO13 samples (20 µL) was injected in an HPLC system (ExionLC, SCIEX) equipped with a reversephase HPLC column (EC 100/2 Nucleodur C18 HTec, 100 × 2 mm ID, 1.8 µm particle size, MachereyNagel, Düren, Germany). The temperature of the column oven was set at 50 °C. The HPLC elution was performed at a flow rate of 0.35 mL min^{-1} in the gradient mode. The mobile phases were an aqueous solution of 2 mM ammonium formate containing 0.05% formic acid (A) and ACN with 0.05% formic acid (B). The initial composition of the gradient was pure A. The proportion of B was then increased to 10% in 12 min, set to 60% at 20 min and reached 100% at 22 min. The latter composition was maintained for 3 min. The outlet of the column was directed first to a UV diode array detector and then to the inlet of a 6500 + QTrap mass spectrometer (SCIEX) operated in the positive electrospray ionization. Single stage mass spectrometry analyses (MS1) were performed with the second analysis quadrupole used a linear ion trap. The mass range was 50 to 1000. Additional experiments were performed in the product ion scan mode (MS2) aimed at recording fragmentation mass spectra of compounds detected in MS1.

Production and purification of a photoproduct of PO13

PO13 was suspended in isopropanol (35 mL) at a concentration of 1 mg mL^{-1}, and the sample was sonicated in a bath sonicator for 20 min. The suspension was transferred in a 75 mL quartz tube containing a 2 cm magnetic bar. It was placed under magnetic stirring in the beam of a XLS1600R3 solar simulator emitting the UV portion of sunlight. The intensity was 3.1 mW cm^{-2}. The irradiated suspension was centrifuged and the supernatant was then filtered at 0.2 µm. The resulting solution was evaporated to dryness in a rotary evaporator. The residue was solubilized in 3 mL of ACN, filtered at 0.2 µm and injected by fractions of 600 µL onto a HPLC system equipped with a reversephase HPLC column (EC 100/2 C18 Nucleosil, 250 × 4 mm ID, 5 µm particle size, MachereyNagel, Düren, Germany). A gradient similar to that used for HPLC-MS/MS analyses was used, with the exception of the flow rate set at 1 mL min^{-1}. The elution was monitored by a UV detector set at 230 nm. A compound eluting as a large peak at 17 min was collected. An aliquot fraction was dried and solubilized into dimethylformamide (DMF) for recording a UVvisible absorption spectrum. It was then compared to that of a 10 µM solution of PO13 in solution. Extensive characterization of the isolated photoproduct was performed by HPLCMS/MS and MS3. For the latter analyses, the solution of photoproduct was introduced with a syringe at a constant flow rate of 10 µl min^{-1} in the 6500 + QTrap mass spectrometer with the third quadrupole used as a linear ion trap. The collision energy for the pseudo molecular ion (m/z 423) in the collision cell was set at 35 eV and the amplitude of the resonant excitation field inducing fragmentation of the second precursor (m/z 330 or 237) in the ion trap was set at AF2 = 0.1.

Cell culture

HaCaT cells (CLS, Eppelheim, Germany), an immortalized keratinocytic cell line, were cultured in high glucose Dulbecco's modified Eagle's medium with Glutamine (DMEM + GlutaMAX™; 31966021, Gibco, Illkirch, France) supplemented with 10% fetal bovine serum (FBS, Gibco), 100 UI/mL penicillin and 0.1 mg mL^{-1} streptomycin (Sigma), and maintained under an atmosphere of 5% CO_2 at 37 °C.

Cell viability assay

On the day prior to the treatment, HaCaT cells were seeded into 96-well plates (2.5×10^4 cells/well) in culture medium. On the next day, 100 µL of suspensions containing different concentrations of PO13 (0.03–30 µg mL^{-1}) was added for 24 h. At the end of the treatment, 3-(4,5-dimethylthiazol-2-yl)−2,5-diphenyltetrazolium bromide (MTT, Sigma) solution was added in order to reach a concentration of 0.45 mg mL^{-1} in each well. After 2 h at 37 °C, medium was discarded and formazan crystals were dissolved in 100 µL DMSO. Absorbance was measured at 550 nm (SpectraMax M2, Molecular Devices). Possible interferences of PO13 with the assay were taken into account by measuring the absorbance in exposure medium without adding MTT for each experimental condition. The obtained values were subtracted from those obtained in the presence of the probe.

Detection of reactive oxygen species by CMH2DCFDA

Production of intracellular ROS content was monitored using CMH_2DCFDA (5(and-6)-chloromethyl-2′,7′-dichlorodihydrofluorescein diacetate, acetyl ester, Invitrogen, France) assay. On the day prior to the treatment, HaCaT cells were seeded into black 96-well plates (3.5×10^4 cells/well) in culture medium. On the next day, cells were rinsed with Dulbecco's Phosphate Buffered Saline (DPBS, Gibco, Illkirch, France) and incubated for 1 h with a DPBS solution containing 5 µM CMH_2DCFDA (Invitrogen) and 0.2% DMSO. As control, wells were only incubated with a DPBS solution containing 0.2% DMSO. At the end of the incubation, cells were rinsed with DPBS. High glucose DMEM without phenol red (31053028, Gibco, Illkirch, France) supplemented with 4 mM GlutaMax (35050061, Gibco), 1 mM sodium pyruvate (S8636, Sigma) and with 10% fetal bovine serum, 100 UI/mL penicillin and 0.1 mg mL^{-1} streptomycin was added in wells, followed by a 45 min incubation. Then, medium was discarded and suspensions containing different concentrations of PO13 (0.003 to 0.3 mg mL^{-1}) were added. As positive control, a solution with 250 µM *tert*Butyl hydroperoxide (tBuOOH, Sigma) was added to wells. After a 4hour treatment, the fluorescence of fluorescein was measured at $\lambda_{exc}/\lambda e_m$ 488 nm/535 nm (SpectraMax M2). Potential interference of pigment particles were taken into account by measuring the fluorescence of cells exposed to PO13 or DCBP incubated with a solution containing 0.2% DMSO without CMH_2DCFDA. The obtained values were subtracted from those obtained in the presence of the probe. Results were normalized by dividing the difference between the measured fluorescence intensity for a specific condition and the mean of that

for the vehicle control by the difference between the mean for the positive control and the mean for the vehicle control. Values are expressed in percent.

Comet assay

On the day prior to the treatment, HaCaT cells were seeded into 12-well plates (3×10^5 cells/well) in culture medium. On the next day, suspensions containing different concentrations of PO13 (0.003, 0.03 and 0.3 µg mL^{-1}) were added and the plates incubated for 24 h. As positive control for the assay, methyl methanesulfonate (MMS) at 30 µg mL^{-1}, was used to induce DNA breaks. At the end of the exposure, medium of wells was discarded. The wells were rinsed with DPBS. Cells were recovered with trypsinEDTA and stored at −80 °C in a storage buffer. The comet assay was performed in its alkaline version. Briefly, microscope slides were coated with 1% normal melting point agarose (NMA) and allowed to dry. Fifty µL of cell suspensions were mixed with 450 µL of prewarmed 1% low melting point agarose (LMPA) and then, 70 µL of these mixture were deposited over the agarose layer, and the LMPA/cells mix was allowed to solidify on ice. After solidification of the gels, the slides were immersed for 1 h in cold lysis solution (2.5 M NaCl, 100 mM EDTA, 10 mM Tris, 1% Triton X-100 with pH 10) in the dark. Slides were rinsed three times with PBS for 5 min. DNA was then allowed to unwind for 30 min in cold alkaline electrophoresis solution (300 mM NaOH, 1 mM EDTA). Electrophoresis was performed in a field of 1.2 V cm^{-1} and 300 mA current for 30 min in the same solution. Slides were rinsed twice with PBS for 10 min. Samples were stained with GelRed (Biotium, San Francisco, USA) for scoring. At last, 50 comets per slide were analyzed under a fluorescence microscope (Zeiss) equipped with a LED emitting light with 380–770 nm wavelength (XCite Xylis, Model No. XT720L, Excelitas Canada Inc., Kitchener, Canada) at ×20 magnification. Percentage of tail DNA was measured by using Comet IV software (Perceptive Instruments, Suffolk, UK).

Quantitative proteomics analysis

Cell treatment and lysis

HaCaT cells were seeded in 6well plates (7.5×10^5cells/well) in culture medium. The next day, a volume of 2 mL of the tested samples was added. Those were: (i) 7 replicates of the vehicle control (1% water in culture medium), 6 replicates of photoaged suspension (96 h, 0.03 µg mL^{-1}) and 3 replicates of the corresponding temperature control; (ii) 5 replicates of filtrates of photoaged suspensions (96 h, 0.3 µg mL^{-1}) and 5 replicates of the corresponding temperature control; and (iii) 5 replicates of 2 µM DCBP and 5 replicates of the solvent control (0.2% DMSO in culture medium). At the end of a 24 h exposure, the supernatant was removed and the wells were rinsed with 2 mL of DPBS containing $CaCl_2$ and $MgCl_2$ (Gibco). DPBS (2 mL) was added and the cells were then gently scraped from the bottom of the wells to be suspended and collected. The cell suspension was centrifuged (300xg, 5min). The supernatant was carefully removed and the pellet was suspended in 1 mL of standard DPBS. The resulting suspension was centrifuged (300xg, 10 min). The supernatant was gently removed and the cell pellet was resuspended in 100 µL lysis buffer (4 M urea, 2.5% hexadecyltrimethylammonium chloride (SigmaAldrich), 150 µM methylene blue, 10% of a phosphate buffer at pH 3). After 30 min at room temperature, the lysed cell suspensions were centrifuged (15,000xg, 15 min). The supernatant was collected and stored at −20 °C.

Sample preparation for nanoLCMS/MS analysis

Solutions of iodoacetamide (IAA), dithiothreitol (DTT) and trypsin were prepared in 25 mM NH_4HCO_3. The protein content of the samples was quantified using the Bradford method in a 96-well plate. The samples were then transformed into gel plugs using a polymerization reaction[26]. A sample containing 10 µg of protein was prepared in 0.5 mL conical tubes for a total volume of 16 µL. A polyacrylamide solution was prepared with 1 mL of a commercial acrylamide/bis-acrylamide 40% solution (Interchim, France), 100 µL of a saturated aqueous solution of diphenyliodonium chloride, 100 µL of a solution of 1 M toluene-4sulfinic acid (Fluka), mixed with 300 µL of water. In a subsequent step, 4 µL of this solution were added to the protein sample. Water-saturated butanol (100 µL) was then added to guarantee hydration of the gel. Polymerization was carried out by exposing the tubes for 2 h to a 1500 lm 2700 K LED lamp. The butanol was then aspirated and the gels transferred to a 96well plate intended for proteomic analysis. The gels were fixed for 1 h with 200 µL of a solution of 20% ethanol and 5% phosphoric acid (SigmaAldrich). The solution was then eliminated and 3 washes of 15 min with a 20% ethanol solution were carried out. The gels were stored at −20 °C. They were then destained using 4 washes of 5 min with 100 µL of a solution of 6.25 mM NH_4HCO_3 and 75% ACN. ACN (60 µL) was added and the samples were left for 5 min for dehydration. A reduction of cysteine residues was carried out by adding 60 µL of 10 mM dithiothreitol. Two 30 min incubations took place, a first at 60 °C then a second at room temperature. Reduced cysteine residues were then alkylated by adding 60 µL of 55 mM iodoacetamide for 20 min in the dark, at room temperature. After dehydrating the gels by adding 120 µL of ACN, the solution was eliminated and the gels were washed three times with a 25 mM NH_4HCO_3 solution left for 5 min before addition of ACN. In the final step, the gels were dehydrated again with 50 µL of ACN left for 5 min, twice. The proteins were digested with 20 µL of modified porcine trypsin 10 ng μL^{-1} (Promega, Madison, United States) overnight, at 37 °C. The generated peptides were then extracted by incubating the samples with 40 µL of 60% ACN for 1 h, with stirring followed by a second extraction with ACN (15 µL) for 10 min. The solvent of peptide extracts were evaporated using a rotavapor and dried samples were solubilised in an aqueous solution containing 0.1% formic acid and 2% ACN in order to obtain a final concentration of 150 ng μL^{-1}.

nanoLCMS/MS analysis

Samples were analyzed by nanoLCMS/MS using a nanoACQUITY UltraPerformanceLC system (Waters Corporation, Milford, USA) coupled to a QExactive Plus mass spectrometer (Thermo Fisher Scientific, Bremen, Germany). The nanochromatographic separation was carried out on a nanoEaseTM M/Z Peptide BEH C18

column (130Å, 250 mm x 75 µm, particle size = 1.7 µm, Waters Corporation, Milford, United States) preceded by a nanoEaseTM M/Z Symmetry C18 trapping column (100Å, 20 mm × 180 µm, particle size 5 µm, Waters Corporation, Milford, United States). The mobile phase was composed of 0.1% formic acid in water (solvent A) and 0.1% formic acid in ACN (solvent B). A volume of 1.5 µL of peptide extract was injected into the precolumn for 3 min at 5 µL min^{-1} (solvent A 99%, solvent B 1%) for desalting and concentration. Elution of the peptides was carried out at a flow rate of 350 nL min^{-1} with a 6–35% linear gradient of solvent B in 58 min. The QExactive Plus operates in datadependent acquisition mode by automatically switching between full MS acquisitions and consecutive MS/MS acquisitions. Full scan MS spectra were collected from 300 to 1800 m/z with a resolution of 70,000 at 200 m/z with an automatic gain control target fixed at 3×10^6 ions and a maximal injection time of 50 ms. The top 10 precursor ions with intensity greater than 2×10^5 ions and charge states ≥ 2 were selected from each MS spectrum for fragmentation by higher energy collisional dissociation. MS/MS spectra were collected at a resolution of 17,500 at 200 m/z with a fixed first mass of 100 m/z, an automatic gain control target fixed at 1×10^5 ions, and a maximum injection time of 100 ms. Dynamic exclusion time was set to 30 s. The normalized collision energy was fixed at 27 V. The complete system was fully controlled by Thermo Scientific™ Xcalibur ™ software. Raw data were converted to .mgf files using the MSConvert tool of ProteomeWizard (v3.0.6090).

Proteomics data processing

In order to identify proteins, MS/MS data were submitted to Mascot database searches (version 2.6.2) (Matrix Science, London, UK) against a database containing all *Homo sapiens*entries from UniProtKB /SwissProt (version 2019_09, 20,410 sequences), to which common contaminants and decoy sequences were added. The database was generated using MSDA software[27]. Spectra were searched with a mass tolerance of 10 ppm for MS data and 0.07 Da for MS/MS data. Trypsin was selected as the enzyme and a maximum of one missed cleavage was allowed. Acetylation of protein ntermini, carbamidomethylation of cysteine residues, and oxidation of methionine residues were set as variable modifications. Identification results generated by Mascot were validated with Proline software[28] (version 2.2, http://proline.profiproteomics.fr). Peptide spectrum matches (PSM) with a pretty rank equal to 1 and a length of at least 7 amino acids were retained. False discovery rate was then optimized to be below 1% at PSM level using the Mascot adjusted Evalue and below 1% at protein level using Mascot standard score. For label free quantification, peptide abundances were extracted with cross assignment between the conditions. The assignment of LCMS series was performed using Loess regression. Crossassignment was performed within groups. Protein abundances were calculated using the sum of the unique peptide abundances normalized at the peptide level using the median. Differential analysis was then carried out using Prostar software[29] (version 1.34.5) with a significance level of 0.05. Imputation of missing values was done using the approximation of the lower limit of quantification by the 2.5% lower quantile of each replicate intensity distribution ("det quantile"). A Limma moderated *t*-test was applied on the dataset to perform differential analysis. The adaptive Benjamini-Hochberg procedure was applied to adjust the p-values and False Discovery Rate (FDR). Identification of affected pathways was performed on the UniProtKB platform (https://www.uniprot.org/id-mapping). Study of the impacted cellular localization was performed with the STRING database version 12.0 (https://string-db.org/) using a *Gene Ontology* approach.

The mass spectrometry proteomics data have been deposited to the ProteomeXchange Consortium via the PRIDE[30] partner repository with the dataset identifier PXD056061 and https://doi.org/10.6019/PXD056061.

Statistics

GraphPad Prism 9 software (Boston, USA) was used for the statistical analyses of data obtained for cell viability, ROS production and Comet assay. KruskalWallis tests followed by Dunn's multiple comparisons were used to analyze data from dosecourse studies. KolmogorovSmirnov tests were applied to the comparison of results arising from different types of samples. Results were considered significant with $p \leq 0.05$.

Results

Characterization of physicochemical properties of PO13 particles by photoaging

The hydrodynamic diameter distribution and the zeta potential of PO13 particles were measured by dynamic light scattering and electrophoretic light scattering, respectively. Pristine pigment, photoaged pigment and temperature control suspensions (i.e. pigment suspension aged in the dark at 40 °C for 96 h) were analyzed. A larger proportion of small particles was detected in aged pigment suspension compared to the temperature control or pristine pigment (Fig. 1). Moreover, pristine pigment suspension contained larger particles than temperature control. The median size was 541, 307 and 174 nm for the pristine, temperature control and photoaged pigments, respectively. The size range for PO13 particles and agglomerates in the two latter types of samples was confirmed by transmission electron microscopy (Supplementary information Fig. S1).

In the three samples, the surface potential of PO13 particles was unequivocally negative. It was -29.2 ± 6.9 mV for the pristine pigment. A slight increase in the absolute value of zeta potential was observed between the temperature control (-39.8 ± 2.5 mV) and photoaged (-46.6 ± 3.6 mV) samples but it remained in the same range.

Characterization of the soluble fraction of photo-aged PO13 suspensions

HPLC-MS analysis of the aqueous fraction

Aqueous suspensions of PO13 were exposed to simulated sunlight and filtered at 0.2 µm. The filtering step had two purposes. The first was to isolate small particles and soluble products from the bulk of the pigment. The aim was to assess the toxicity of degradation products. The other point was more practical and was to prevent injection of particles that could clog the HPLC columns. The 0.2 µm threshold was found to be efficient since a colorless filtrate was obtained and the pigment remained on the filter. Filtrates were analyzed by HPLC-MS to

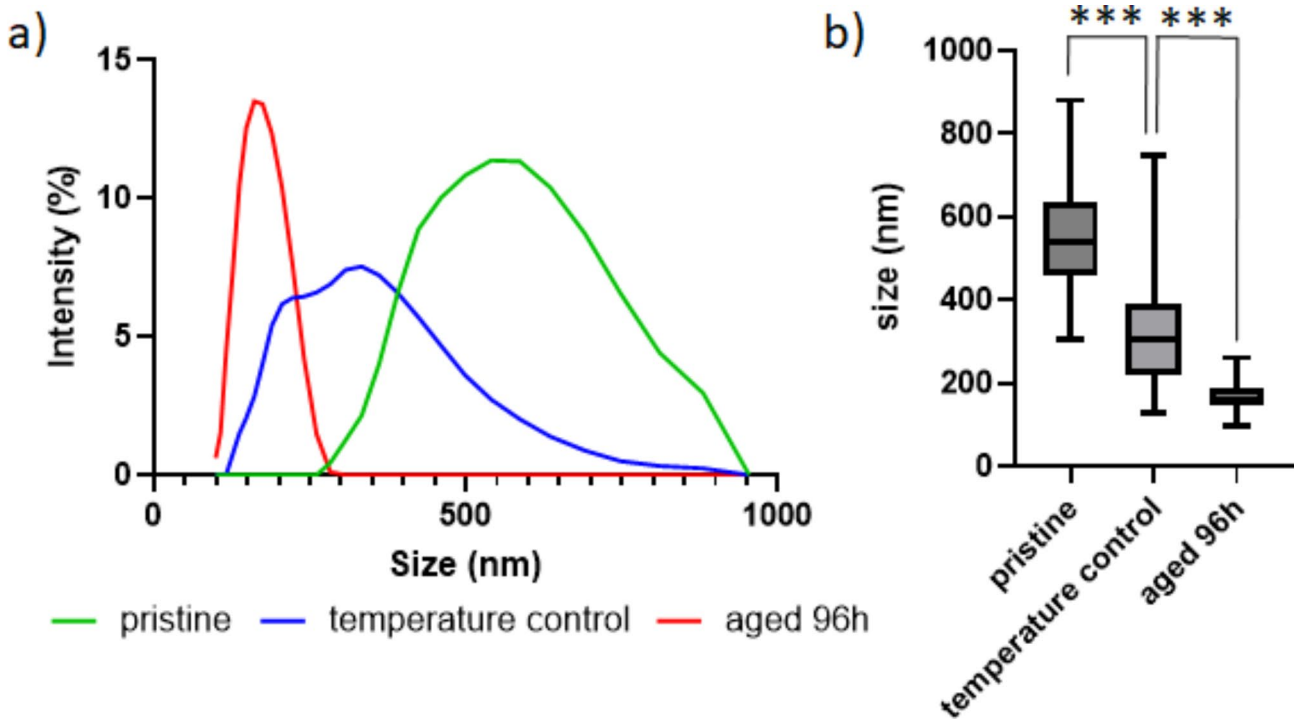

Fig. 1. Size distribution of PO13 particles either under their pristine form, after incubation for 96 h in the dark (temperature control) or photo-aged in a climate chamber: (a) distribution of the three sample types (mean of at least 3 independent experiments) and (b) comparison of the median hydrodynamic diameters. The concentration during treatment was 10 mg mL^{-1}. The reported results in b) were expressed as the median, the first and third quartiles and the minimum and maximum values of at least three independent experiments. The statistical significance between each samples relied on a nonparametric Kolmogorov Smirnov test (*** $p < 0.001$).

monitor photodegradation of the pigment into photoproducts. Chromatograms indicated the formation of new products. A first run was performed in single stage mass spectrometry in order to identify the pseudomolecular ions of components of the mixture over a large range of m/z values (50–1000). Chromatograms generated upon analysis of photoaged suspensions were compared to those of the control temperatures, which allowed to identify potential photoproducts. A second analysis was then performed in the MS2 mode to collect fragmentation mass spectra of the pseudomolecular ions of the compounds of interest identified in the MS1 analysis. This provided information that could help us to propose structures of the putative photoproducts. In addition, integration of the peaks of interest on the MS2 chromatograms provided semiquantitative information of the timecourse formation of the compounds of interest. We thus identified photoproducts that were only transiently produced, while others, more interesting in terms of longterm toxicity of pigments, were accumulated upon photoaging (Supplementary Information Fig. S2).

HPLC-MS analysis of the octanol extracts

In addition to the filtrate of the aqueous suspension, we performed HPLC-MS/MS analysis of an octanol extract of the pellet of photo-aged suspension. Some products were detected in small amounts at different time points but one was in larger amounts than the other. It was produced in a time-dependent manner (Fig. 2a). Its long retention time (20.1 min) showed that it was highly hydrophobic, which could explain why it was not detected in aqueous fractions. The pseudo-molecular ion on the MS1 spectrum exhibited an isotopic distribution with a series of pseudo molecular ions centered at m/z = 424 with a typical isotopic distribution of a molecule bearing 2 chlorine atoms (one ion at m/z = 423 and one at m/z = 425 in 1.5:1 ratio) (Fig. 2b).

Isolation and characterization of a photoproduct (DCBP)

In order to prepare larger amounts of the photoproduct detected in the octanol extracts of photo-aged PO13 aqueous suspensions, we exposed a large volume of suspension (35 mL) in isopropanol, an organic solvent making possible a more stable suspension than in water. In addition, we used a UV solar simulator more powerful than the climate chamber. Last, the duration of exposure was longer than the 4 days used in photo-aging. Formation of soluble photoproducts was monitored by HPLC-MS and UV absorption. Several peaks were observed on the chromatograms during the first 48 h. The corresponding products either decomposed or reached a maximum yield at that time. Only one compound eluting at 20.1 min was detected in increasing amount, by both UV absorption and mass spectrometry, from the shortest to the longest exposure time (160 h). The retention time and the MS1 mass spectrum were identical to those of the photoproduct detected in octanol

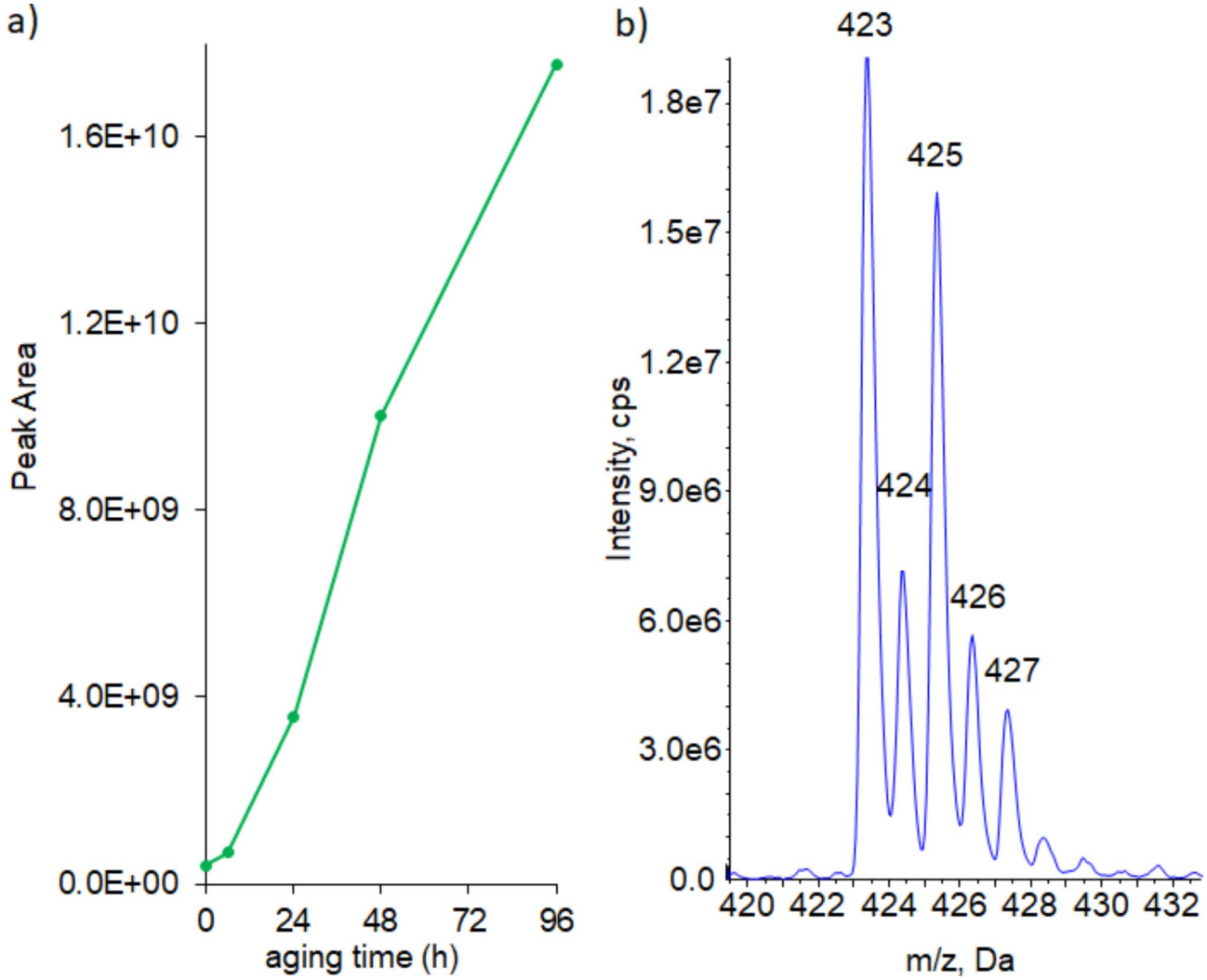

Fig. 2. Detection of a photoproduct in the octanol extract of photo-aged PO13 pigment (a) time course formation in photoaged aqueous suspensions of PO13, (b) pseudo-molecular ion observed on the MS1 mass spectrum.

extract of PO13 photo-aged in water. Extensive mass spectrometry characterization strongly suggested that the isolated photoproduct was 4((3,3'dichloro-[1,1'biphenyl]−4yl)diazenyl)−5methyl-2phenyl-2,4dihydro-3Hpyrazol-3one (DCBP, Fig. 3a), which would arise from the cleavage of one of the diazo groups with loss of one of the 5-methyl-2phenyl-2,4-dihydro-3-H-pyrazol-3-one units of PO13 (Fig. 4). As explained above, the photoproduct exhibited a mass spectrum with a isotopic distribution typical of a molecule bearing 2 chlorine atoms (one ion at m/z = 423 and one at m/z = 425 in 1.5:1 ratio). The MS2 and MS3 mass spectra (Supplementary Information Fig. S5), were in agreement by the fragmentation of the photoproduct into of a triazolo-cinnoloin derivative upon loss of aniline and of dichloro-dibenzofuran after loss of the 5-methyl-2-phenyl-pyrazolone unit. It may be added that the UV-visible absorption spectrum of the photoproduct in DMSO exhibited a peak at 418 nm, while the starting PO13 had a maximal absorption at 478 nm. This blue shift is in agreement with the loss of conjugations in the photoproduct.

Toxicological profile of photo-aged PO13 in a keratinocyte model

Effect of photoaging of PO13 on cell viability

HaCaT cells were exposed to photoaged PO13 suspensions or temperature controls at different concentrations for 24 h. At the end of the treatment, cell viability was measured by a MTT assay (Fig. 4a). A significant decrease in HaCaT viability was detected for concentrations larger than 0.3 µg mL^{-1} for photoaged PO13 ($p < 0.01$) and 3 µg mL^{-1} for temperature controls ($p < 0.001$). A significant lower viability for photoaged PO13 compared to temperature control was only observed at 0.03 µg mL^{-1} ($p < 0.001$). It should yet be stressed that, at this concentration, the viabilities were not significantly different from that measured for the vehicle control (1% water in the medium).

HaCaT cells were also treated with the soluble fraction of aged suspensions obtained by 0.2 µm filtration. Cells were exposed for 24 h to increasing concentrations of filtrate corresponding to the various conditions used to test

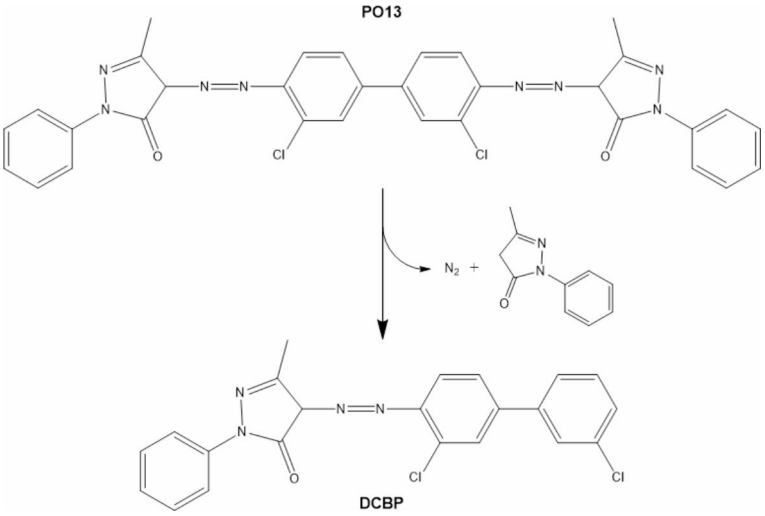

Fig. 3. Proposed chemical structure and mechanism of formation of DCBP upon photodegradation of PO13.

the toxicity of whole PO13 suspensions (Fig. 4b). A statistically significant decrease in cell viability compared to the control was measured for the filtrate of photoaged suspensions at 3 µg mL^{-1} and 30 µg mL^{-1}, while no effect was observed for the temperature controls. More interestingly, the filtrate of photoaged PO13 suspensions induced a significantly larger loss of viability than the temperature control for the three concentrations larger than 0.3 µg mL^{-1}.

Production of ROS and induction of DNA breaks by photoaged PO13

We did not observe induction of DNA strand breaks by the alkaline Comet assay (Supplementary Information Fig. S3a) upon exposure of HaCaT cells to either the control or photo-aged suspensions, or their filtrates. The potential of PO13 to induce ROS in HaCaT cells was also investigated by CM-H_2DCFDA assay (Supplementary Information Fig. S3b). After 4 h treatment, it was not possible to detect an increase in DCF fluorescence intensity with the different tested PO13 concentrations regardless experimental conditions whereas the positive control was able to induce this cellular response.

Impact of aged PO13 on the proteome of HaCaT cells

The impact of photoaged PO13 on the keratinocyte proteome was investigated by global differential proteomics. Seven replicates were used for the vehicle control, 3 for the temperature control and 6 for the photo-aged suspension. Over the 2950 quantified proteins, 2502 proteins were present in at least 80% of the samples for a same condition and were kept for differential analysis. Because the impact of PO13 samples was limited, we did not use a very stringent value for the threshold of significant modulation. The p-value was set at 0.05, which led to a rather high FDR (76.8%). Under these conditions, 73 proteins were identified as modulated by PO13 exposed to simulated sunlight compared to vehicle control. Compared to temperature control, 149 proteins were identified as modulated by photoaged PO13. The dendrogram representing the relative expression of proteins in every sample was not able to cluster samples by experimental condition. The associated heatmap showed that the proteome was not strongly different between the different conditions (Fig. 5). A similar approach was applied to the identification of the putative effects of filtrates of photo-aged suspensions. Five replicates of filtrates-treated cells and 5 replicates of corresponding temperature controls were included. A total of 2481 proteins were quantified in the different samples. Like for the whole suspension, the heatmap did not reveal differences between the treated samples and their controls (Supplementary Information Fig. S4). Nevertheless the differential analysis between the aged samples and their temperature controls led to the identification of 62 differentially expressed proteins (p-value 0.05, FDR = 95.5%).

Among the 149 proteins modulated upon exposure to photo-aged suspensions, biological pathways common to several proteins were identified. Indeed, ASAH1, SPTC2, PGES2 and AGK are involved in lipid metabolism. UMPS, HRPT and APT have a role in pyrimidine and purine metabolism, respectively. They were all three overexpressed in HaCaT cells treated with aged PO13 compared to temperature control. CUL2 and UBR4 involved in protein ubiquitination are also overexpressed (Supplementary Information Table S1). The same pathways were found to be modulated when cells were exposed to the filtrates.

Toxicological profile of the PO13 photoproduct DCBP in a keratinocyte model

Toxicological properties of DCBP

HaCaT cells were treated for 24 h with different concentrations of the photoproduct and then, a MTT assay was performed. Compared to vehicle control, HaCaT viability was significantly reduced for concentrations larger than 2 µM ($p < 0.01$; Fig. 6). At these concentrations, DCBP was also found to significantly induce the production of ROS in HaCaT cells (Fig. 7a). In contrast, it did not induce DNA strand breaks at the tested

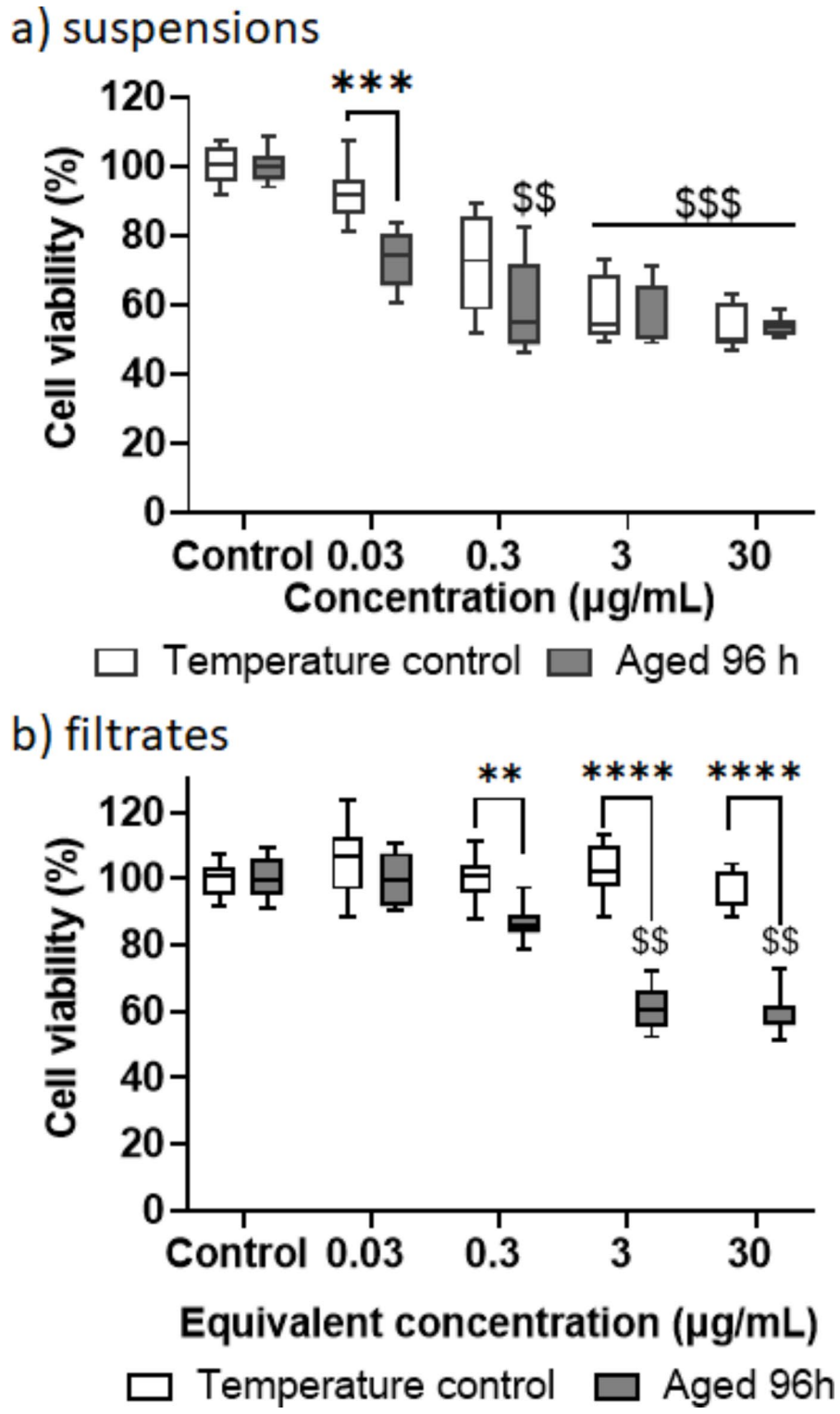

Fig. 4. Effects of photoaging on the impact of PO13 on viability. (a) HaCaT cells were treated with aged PO13 suspensions or their temperature controls at different concentrations (0.03–30 µg mL^{-1}) and water (1%) as vehicle control. (b) HaCaT were treated with filtrates of the latter samples for 24 h. Reported equivalent concentrations are the concentrations of the photoaged suspension used to prepare the filtrate. Results were expressed as the median, the first and third quartiles and the minimum and maximum values. $ indicates significant differences from vehicle control (KruskalWallis test followed by Dunn's multiple comparisons, $$ $p < 0.01$, $$$ $p < 0.001$). * indicates significant differences between aged PO13 and temperature control at the same concentration of pigment (KolmogorovSmirnov test, ** $p < 0.01$, *** $p < 0.001$, **** $p < 0.0001$).

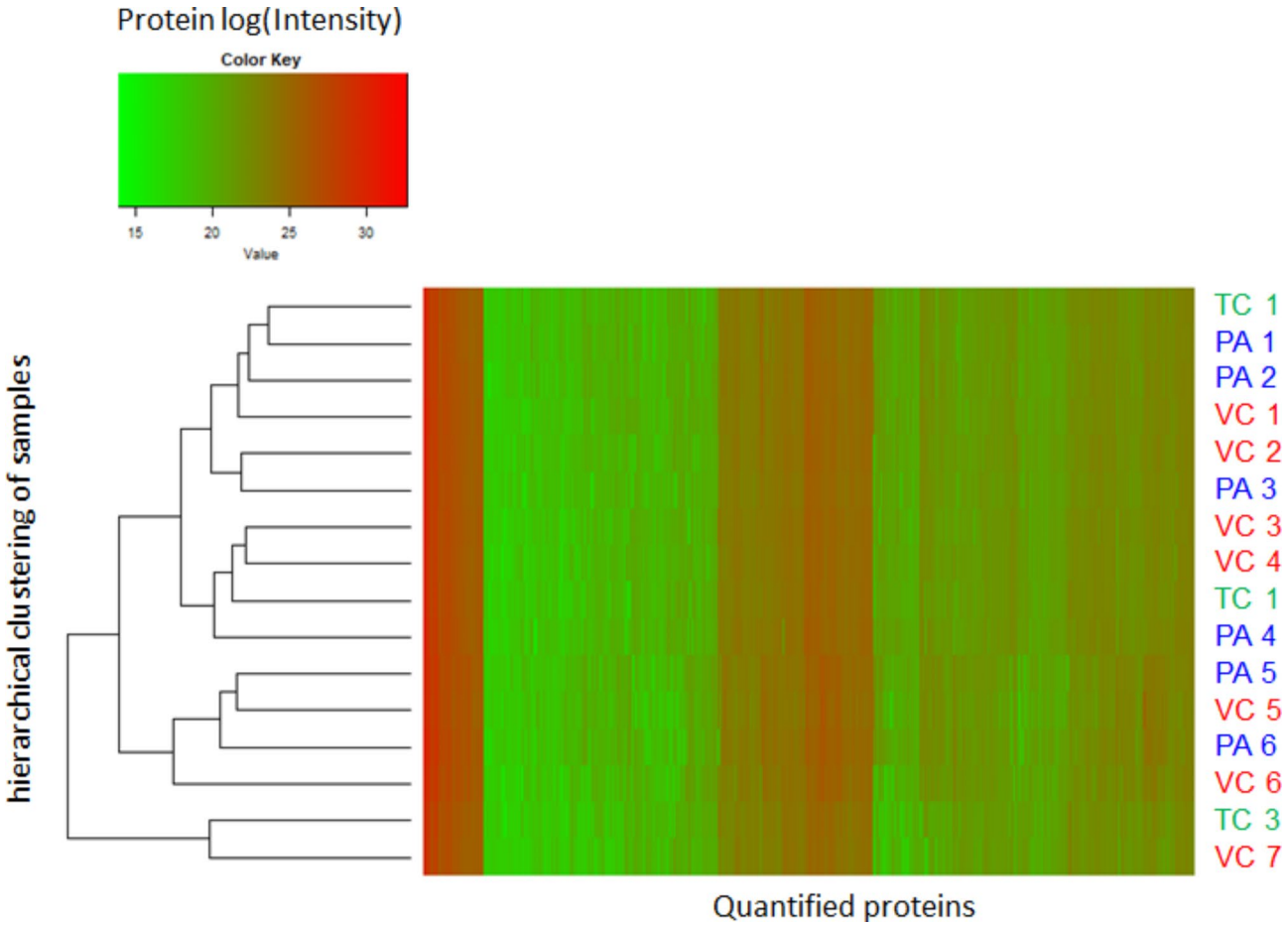

Fig. 5. Heatmap and dendrogram of PO13 samples. HaCaT cells were treated for 24 h with aged PO13 suspension, its temperature control (0.03 µg mL^{-1}) or water (1%) as vehicle control. Proteomic data were treated using Prostar software. PA: Photo-aged pigment; TC: temperature control and VC: vehicle control.

concentration of 2 µM (Fig. 7b). Harsher conditions were not investigated because of the cytotoxicity must be limited to 20% in the Comet assay.

Modulation of protein expression by DCBP

The proteomics investigation was based on 6 replicates of cells exposed to the solvent control and 6 replicates treated with DCBP. These analyses led to the quantification of 2487 proteins. The heat map exhibited some level of clustering of the solvent controls and the DCBP-treated samples (Supplementary Information Fig. S6). Difference in protein expression was yet limited. Two hundred proteins were modulated by DCBP below the threshold of $p < 0.05$. Many were underexpressed (156) but with a low foldchange. Other proteins were overexpressed (44). Analysis of pathways for which at least two proteins were modulated showed that several cellular functions were affected by DCBP (Supplementary Information Table S2). In contrast to what was observed with PO13 suspensions, the trend was more at underexpression than overexpression. In addition to the metabolism of lipids, pyrimidines and proteins impacted by PO13, additional pathways were modulated by the photoproduct, namely gluconeogenesis and metabolic activities. An impact of DCBP on metabolism was shown by the modulation of the expression of CYP450 monooxygenases (Fig. 8). CP1A1, which was hardly detectable in controls, was heavily expressed in the presence of DCBP, leading to a fold change of more than 640. Similarly, CP1B1, exhibited a fold change of more than 130 in DCBP-treated HaCaT cells compared to the solvent control. The p value was below 10^{-8} for both proteins. We also analyzed the proteomics data in order to identify the most impacted cellular localizations (Table 1). A large number of proteins exhibiting modulated expression were found in mitochondria, either in the respiratory chain or the nucleoid.

Discussion

In the present work, we addressed the question of the long-term effects of tattoo's pigments. We were in particular interested in the possible formation of low molecular weight degradation products of pigments that could diffuse from the dermis to the epidermis. Among possible degradation pathways, we focused the present investigation on environmental factors such as temperature and solar radiation. The work was performed on PO13, a pigment exhibiting a diazo structure. This chemical feature was a first reason of the choice because diazo compounds have

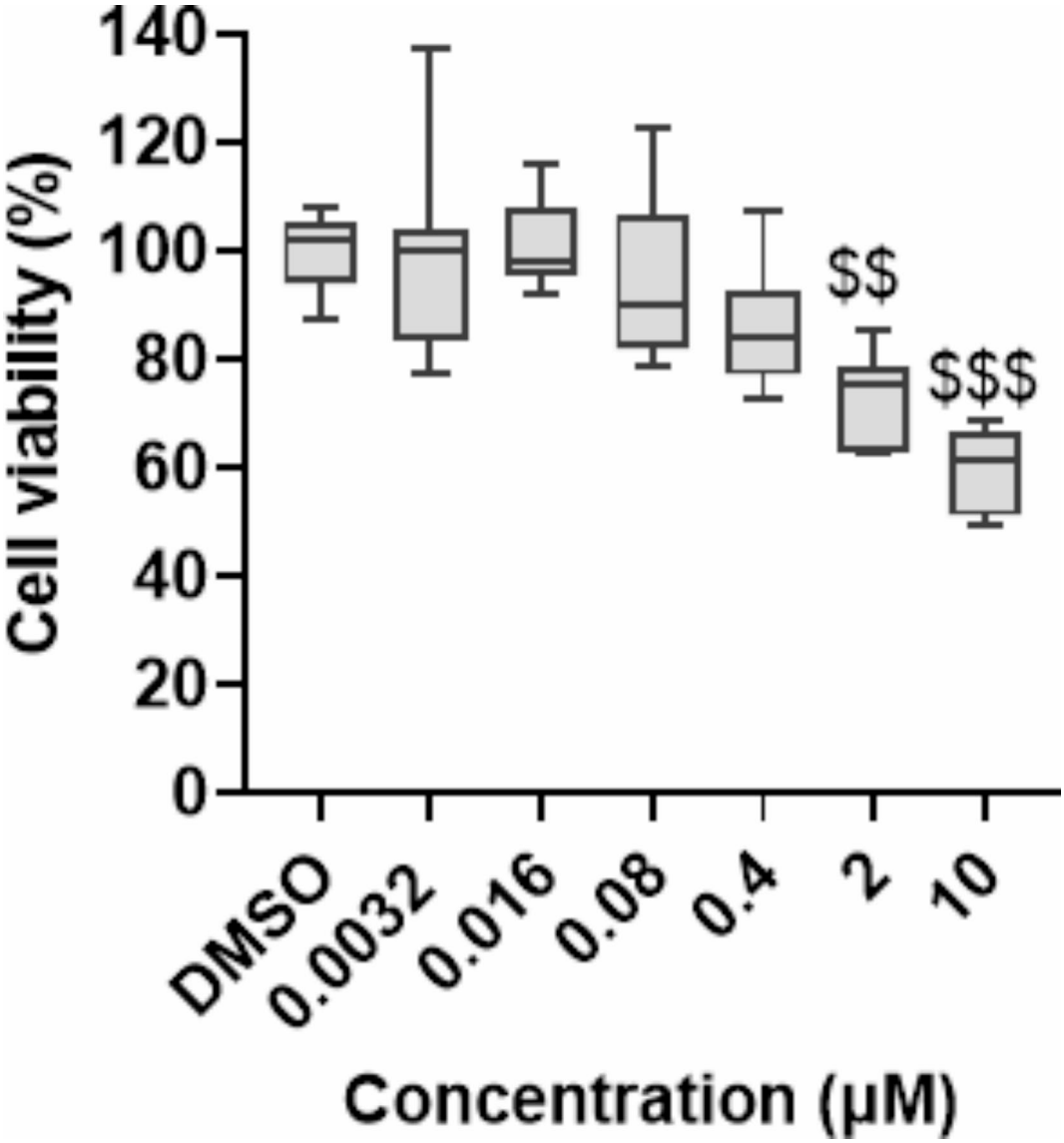

Fig. 6. Effect of DCBP on cell viability of a keratinocyte model. HaCaT cells were treated at different concentrations of the product (0.0032–10 µM) and DMSO (0.2%) as vehicle control. Results were expressed as the median, the first and third quartiles and the minimum and maximum values. $ indicates significant differences from vehicle control (KruskalWallis test followed by Dunn's multiple comparisons, $ $p < 0.05$, $$ $p < 0.01$, $$$ $p < 0.001$).

been reported to generate toxic aromatic amine derivatives[17,31]. Another basis of the study of PO13 is that this compound has been used in tattooing until the very recent limitation enforced by EU regulation, and can thus still be found in current tattoos[4]. Last, we found that PO13 was found to be one of the most cytotoxic to HaCaT in a series of 7 pigments of various types (Supplementary Information Figure S7).

In our work, PO13 was aged by exposure to temperature and solar radiation in a test chamber usually used for the assessment of the degradation of materials. We used this equipment to induce accelerated aging of aqueous suspension of the pigment. In contrast to other works, we did not use organic solvents to be under more physiological conditions. It may be added that the suspensions of PO13 were poorly stable in the presence of PBS, citrate, phosphate and other classical buffers. This led us to use pure water as a medium for the suspension. Physicochemical characterization showed that the PO13 particles were modified by the photoaging treatment, and in particular in terms of diameter. DLS measurements showed that aging aqueous suspensions for 96 h at 40 °C led to a reduction by a factor of 2 of the hydrodynamic diameter. This process was worsened by simulated solar light that generated particles of less than 200 nm diameter, namely three times smaller than those found in the pristine product. In contrast, no significant impact of aging was found on the zeta potential, suggesting that the degraded particles exhibited a structure similar to the initial pigment. Interestingly, TEM imaging revealed that PO13 pigment was composed of agglomerates exhibiting a size in the range of a few hundreds of nanometers. The primary particles of these agglomerates were between 50 and 200 nm long. This

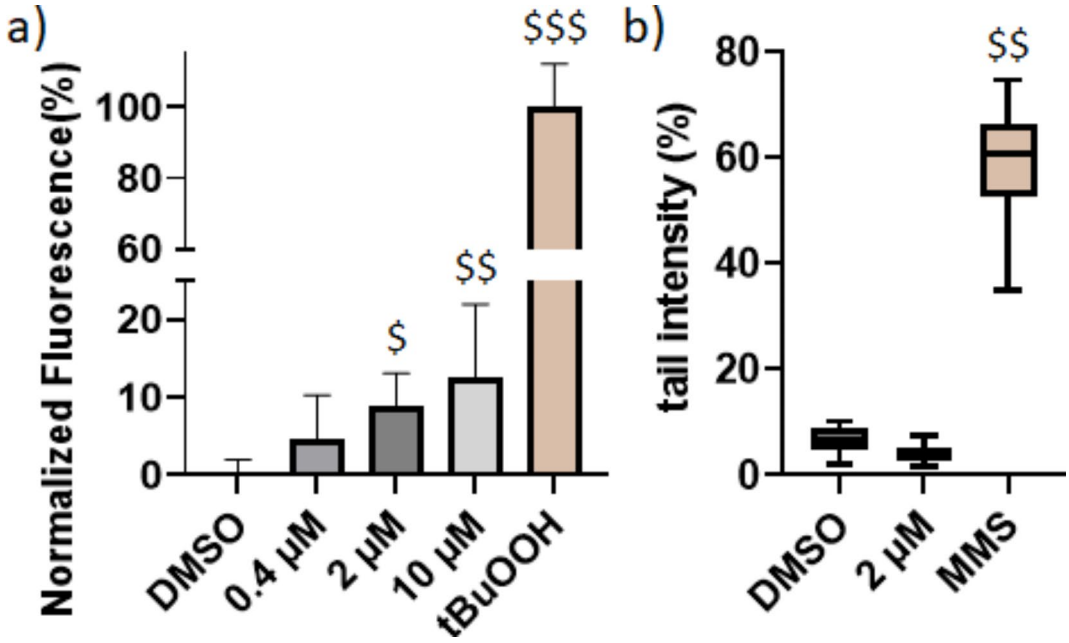

Fig. 7. Detection of (a) ROS and (b) DNA strand breaks in HaCaT cells exposed to DCBP. Three concentrations (0.4, 2 and 0.10 µM) were tested for 4 h for ROS detection. Only one condition was investigated for the Comet assay (2 µM for 24 h). tBuOOH (250 µM) and MMS (30 µg mL^{-1}) were used as the respective positive controls, while DMSO (0.2%) was used as vehicle control. Results were expressed as the median of percentage of DNA in comet tails with the first and third quartiles and the minimum and maximum values. $ indicates significant differences from vehicle control (KruskalWallis test followed by Dunn's multiple comparisons, $ $p < 0.05$, $$ $p < 0.01$, $$$ $p < 0.001$).

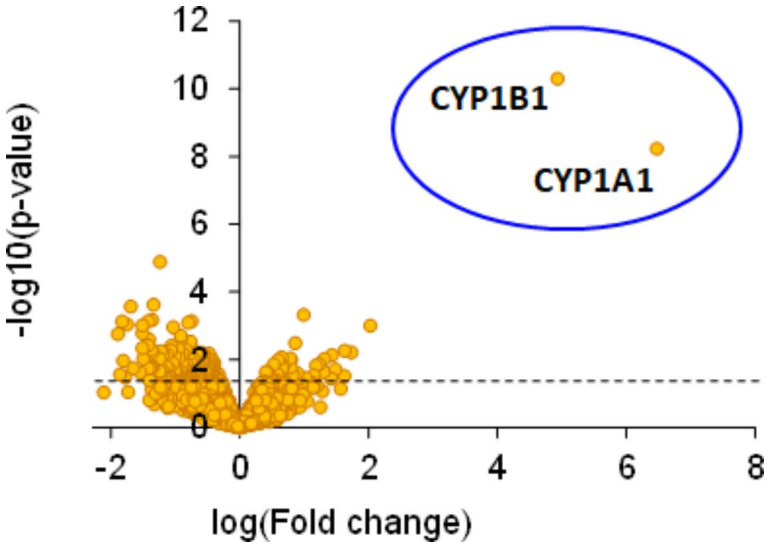

Fig. 8. Volcanoplot of differential analysis of the protein expression between HaCaT cells exposed for 24 h to either DCBP (2 µM) or DMSO (0.2%) as solvent control. After treatment of the proteomic data, differential analysis was performed using Prostar to compare protein expression between the two conditions. The significance level (pvalue of 0.05) is represented by the dashed line. On the left and the right of the yaxis, the protein are under- and overexpressed in cells exposed to DCBP, respectively. CYP1B1 and CYP1A1 appear as the most affected proteins.

observation strongly suggests that the nanosize particles released upon photo-aging are unlikely to arise from the decomposition of PO13 pigments, but rather from a de-agglomeration process. Indeed, the size of the particles present in photo-aged sample is similar to that of the primary particles observed in the agglomerates of pristine suspensions. Whatever the origin of these small particles, they may be involved in the impact of aged

Proteins	Fold change	*p*-value	Cellular component (gene ontology)
FXRD1	1.69	0.014	Complex I of the mitochondrial respiratory chain
NDUV1	0.22	1.65E-03	
NDUB1	0.26	2.41E-04	
NDUS8	0.24	0.018	
NDUA8	0.47	0.012	
NDUA5	0.58	7.60E-03	
NU1M	0.33	0.031	
PPIE	7.57	9.99E-04	U2-type catalytic step 2 spliceosome
RU2A	0.58	0.021	
PRP19	0.55	0.024	
SNW1	1.53	0.023	
SODM	0.59	0.034	Mitochondrial nucleoid
CLPX	0.61	0.017	
LRC59	0.48	0.016	
LPPRC	0.63	0.017	
ODB2	0.58	0.045	

Table 1. Modulation of protein expression after exposure of HaCaT cells to DCBP and grouped according to cellular components by gene ontology. Red and green indicate overexpressed and underexpressed proteins, respectively.

tattoos. Indeed, nanoparticles are known to diffuse in the skin and may thus reach the epidermis[32]. Another conclusion is the significant effect of solar light on pigment integrity. This may be expected since, because of its highly conjugated chemical structure, PO13 efficiently absorbs both UV and visible radiations, which may trigger photochemical degradation processes, as proposed for other pigments[15,18,24].

We next asked the question of the formation of soluble photoproducts. For this purpose, the aged suspensions were filtered at 0.2 µm and the soluble fractions collected. A first characterization step was the recording of a UV-visible absorption spectrum. The suspension was solubilized in DMF to allow a comparison with native PO13, which is difficult to solubilize in other solvents. We observed the presence of absorption bands for the filtrates of aged suspension that were different from of those present in the absorption spectrum of PO13. This observation showed that aging not only fragmented the pigment agglomerates and released small particles, but also generated new soluble molecular photoproducts. This fact was confirmed by analyses involving HPLC-MS. A few additional peaks were observed on the chromatograms of temperature controls compared to filtrate of pristine suspension. In contrast, a large number of new products were detected in samples of PO13 aged in the presence of simulated sunlight. The mass spectrometry information allowed us to determine the molecular weight of some photoproducts and fragmentation data also made possible to propose putative structures. Timecourse data showed that some photoproducts were present only at the beginning of the aging process and then disappeared, likely because of the occurrence of secondary degradation reactions. In contrast, other photoproducts were stable and were accumulated in the aged suspensions during the whole exposure period. Altogether, photodegradation of PO13 appears to be a likely source of soluble photoproducts.

Evidence for the formation of a specific hydrophobic photoproduct in photo-aged aqueous suspensions was in particular obtained upon analysis of an octanol extract of the pigment pellet. Unfortunately, the amounts generated in the aging experiments involving aqueous suspensions did not permit the isolation of this photoproduct. We thus photodegraded PO13 in suspension in isopropanol using a more intense UV source than the aging chamber. Increased degradation in organic solvents has been previously successfully applied to other pigments such as PY74 and made possible the identification of degradation products[15]. The rationale for the use of organic rather than aqueous suspensions is first that a better dispersion of the pigment particles can be achieved. In addition, the photoproducts may more easily remain in solution than in water where hydrophobic interactions may keep them adsorbed onto the particles. We were thus able to isolate a few hundreds of micrograms of the main photoproduct of PO13. Extensive mass spectrometry characterization showed that it arose from the cleavage of one diazo group, leading to the release of 4-((3,3'dichloro-[1,1'biphenyl]−4yl)-diazenyl)−5-methyl-2phenyl-2,4-dihydro-3-H-pyrazol-3one (DCBP). It is worth noting that, unlike a previous study on the aging of a tattoo ink containing PO13 by natural light with UVB part partially blocked, we did not find carcinogenic 3,3′-dichlorobenzidine in our aged samples[17]. This could be explained by the difference of light source and the fact that we used a pure pigment instead of ink.

The importance of photochemically induced processes was confirmed in cellular toxicity experiments. We observed that PO13 kept in the dark exhibits some cytotoxicity on HaCaT cells, for concentrations larger than 3 mg mL^{-1}. Interestingly, suspensions aged in the presence of simulated sunlight were statistically significantly more toxic than these temperature controls at 0.3 and 0.03 mg mL^{-1}. These two results showed that the degradation of PO13 by combined exposure to temperature and light increased its cellular toxicity. A role of the soluble fraction was then observed when the impact of filtrates on viability was studied. No loss of viability was observed in HaCaT cells exposed to the filtrates of the suspensions aged in the dark. In contrast, filtrates

were more cytotoxic than the solvent control when they were prepared from suspensions aged in the presence of artificial sunlight at a concentration above 3 mg mL^{-1}. This filtrates were also more toxic than the filtrates of the temperature control for suspensions concentration above 0.3 mg mL^{-1}. The underlying cellular mechanisms remain yet to be identified. In experiments carried out under conditions leading to limited loss of viability, no evidence could be obtained for the induction of oxidative stress or genotoxicity. In addition, the modulation of the proteome was weak and was not clearly linked to specific cellular responses.

The cellular impact of filtrates prompted us to further investigate the role of low molecular weight soluble photoproducts, in particular DCBP. Availability of a calibrated solution of pure DCBP allowed us to perform specific toxicological studies. DCBP was first shown to induce loss of viability of HaCaT cells at concentrations larger than 2 µM. In the same concentration range, DCBP also led to the release of ROS but without inducing DNA strand breaks. Another interesting cellular effect of DCBP was shown by the proteomic study. Several proteins were under or overexpressed upon treatment with DCBP. Among the induced enzymes, the most drastic effect was observed for CYP1A1 and CYP1B1. This observation shows that DCBP is able to induce AhR-dependent metabolism. Such a result can be explained by its highly aromatic chemical structure, which is a common feature of xenobiotics recognized by the AhR pathway[33,34]. This pathway has been extensively studied in liver but is also induced in skin[35,36]. The induction of CYP1A1 and CYP1B by DCBP could impact the toxicological effect of other compounds such as polycyclic aromatic hydrocarbons, for example in terms of genotoxicity[37]. Exposure to mixtures of PAHs triggering metabolism through the AhR pathway have been found to either potentiate or inhibit the DNA damaging effect of benzo[a]pyrene in several cell types[38–41]and human skin[42]. It is therefore likely that DCBP will disturb metabolism of xenobiotics in tattooed skin. The effect of the photoproducts of PO13 is reminiscent of the reported metabolism of PY74 through the AhR pathway[43], showing the relevance of the latter mechanism to the toxicity of tattoos. Another interesting information provided by the proteomics analysis was the impact of DCBP on mitochondria. This result is in line with the observation of the induction of oxidative stress in cells exposed to this PO13 photoproduct.

Concluding remarks

Our work unambiguously showed that PO13 can be degraded by heat and more importantly by simulated sunlight. A consequence of these processes is an increase of its toxic potential. We also showed that the liquid phase of the photo-aged suspensions was cytotoxic and contained photoproducts. One of the most abundant, DCBP, was isolated and found to be cytotoxic. Further studies are necessary to confirm that the results obtained here *in vitro* also take place in more biologically relevant and in whole skin. In that respect, the identified soluble toxic photoproducts could be a useful biomarker in human studies. The strategy defined in this work is currently applied in our group to the degradation of PO13 in phagolysosome and to the environmental aging of other organic pigments.

Data availability

The mass spectrometry proteomics data have been deposited to the ProteomeXchange Consortium via the PRIDE partner repository with the dataset identifier PXD056061 and 10.6019/PXD056061. Other data supporting the findings of this study are available within the paper and its Supplementary Information, or will be sent on request to the corresponding author.

Received: 23 September 2024; Accepted: 17 December 2024
Published online: 03 January 2025

References

1. Kluger, N., Seité, S. & Taieb, C. The prevalence of tattooing and motivations in five major countries over the world. *J. Eur. Acad. Dermatol. Venereol.* **33**, e484–e486 (2019).
2. Engel, E. et al. Modern tattoos cause high concentrations of hazardous pigments in skin. *Contact Dermat.* **58**, 228–233 (2008).
3. Baranska, A. et al. Unveiling skin macrophage dynamics explains both tattoo persistence and strenuous removal. *J. Exp. Me.* **215**, 1115–1133 (2018).
4. European Commission (EU). Commission Regulation Amending Annex XVII to Regulation (EC) No 1907/2006 of the European Parliament and of the Council Concerning the Registration, Evaluation, Authorisation and Restriction of Chemicals (REACH) as Regards Substances in Tattoo Inks or Permanent Make-Up. vol. 2020/2081. (2020).
5. Ly, T. & Lee, S. If you think you can safely ink, beware of the masking effects of tattoos. *Hong Kong J. Dermatol. Venereol.* **20**, 106–110 (2012).
6. Laux, P. et al. A medical-toxicological view of tattooing. *Lancet* **387**, 395–402 (2016).
7. Serup, J., Carlsen, K. H. & Sepehri, M. Tattoo complaints and complications: diagnosis and clinical spectrum. *Curr. Probl. Dermatol.* **48**, 48–60 (2015).
8. Wenzel, S. M., Rittmann, I., Landthaler, M. & Bäumler, W. Adverse reactions after tattooing: review of the literature and comparison to results of a survey. *Dermatology* **226**, 138–147 (2013).
9. Bendsoe, N., Hansson, C. & Sterner, O. Inflammatory reactions from organic pigments in red tattoos. *Acta Derm Venereol.* **71**, 70–73 (1991).
10. van der Bent, S. et al. a. s. Complications of tattoos and permanent makeup: overview and analysis of 308 cases. *J Cosmetic Dermatol* 20, 3630–3641 (2021).
11. Hutton Carlsen, K. & Serup, J. Photosensitivity and photodynamic events in black, red and blue tattoos are common: a 'Beach Study'. *J. Eur. Acad. Dermatol. Venereol.* **28**, 231–237 (2014).
12. Negi, S. et al. Benzo(Ghi)perylene (BgP) a black tattoo ingredient induced skin toxicity via direct and indirect mode of DNA damage under UVA irradiation. *Chem. -Biol Interacti.* **379**, 110508 (2023).
13. Kluger, N. & Koljonen, V. Tattoos, inks, and cancer. *Lancet Oncol.* **13**, e161–e168 (2012).
14. Leijs, M. et al. Cutaneous malignancies in tattoos, a case series of six patients. *Curr. Oncol.* **28**, 4721–4737 (2021).
15. Cui, Y. Y. et al. Photodecomposition of Pigment Yellow 74, a pigment used in tattoo inks. *Photochem. Photobiol.* **80**, 175–184 (2004).

16. Engel, E. et al. Tattooing of skin results in transportation and light-induced decomposition of tattoo pigments – a first quantification in vivo using a mouse model. *Exp. Dermatol.* **19**, 54–60 (2010).
17. Hauri, U. & Hohl, C. Photostability and breakdown products of pigments currently used in tattoo inks. *Curr. Probl. Dermatol.* **48**, 164–169 (2015).
18. Engel, E. et al. Photochemical cleavage of a tattoo pigment by UVB radiation or natural sunlight. *JDDG: J. Der Deutschen Dermatologischen Gesellschaft*. **5**, 583–589 (2007).
19. Sepehri, M., Sejersen, T., Qvortrup, K., Lerche, C. M. & Serup, J. Tattoo pigments are observed in the Kupffer cells of the liver indicating blood-borne distribution of tattoo ink. *Dermatology* **233**, 86–93 (2017).
20. Schreiver, I., Hutzler, C., Laux, P., Berlien, H. P. & Luch, A. Formation of highly toxic hydrogen cyanide upon ruby laser irradiation of the tattoo pigment phthalocyanine blue. *Sci. Rep.* **5**, 12915 (2015).
21. Bauer, E. M. et al. Treatments of a phthalocyanine-based green ink for tattoo removal purposes: generation of toxic fragments and potentially harmful morphologies. *Arch. Toxicol.* **94**, 2359–2375 (2020).
22. Devcic, J. et al. Immediate and Sustained effects of cobalt and zinc-containing pigments on macrophages. *Front. Immunol.* **13**, (2022) Article 865239
23. Scalia, S., Dozzo, A., Magli, S. & Scarcella, G. Incorporation in lipid microparticles of Acid Red 87, a colorant used in tattoo inks: effect on photodegradation under simulated sunlight and laser radiation. *Photochem. Photobiology*. **96**, 998–1004 (2020).
24. Fraser, T. R., Ross, K. E., Alexander, U. & Lenehan, C. E. Current knowledge of the degradation products of tattoo pigments by sunlight, laser irradiation and metabolism: a systematic review. *J. Expo Sci. Environ. Epidemiol.* **32**, 343–355 (2022).
25. International Organization for Standardization (ISO). Plastics — Methods of exposure to laboratory light sources Part 2: Xenon-arc lamps, ISO 4892-2:2013. (2023).
26. Muller, L., Fornecker, L., Cianferani, S., Carapito, C. & Tube-Gel A Fast and effective sample preparation method for high-throughput quantitative proteomics. in *Methods in Molecular Biology. Proteomics for Biomarker Discovery* (eds. Brun, V. & Couté, Y.) vol. 123–127 (Springer New York, New York, NY, 2019). (1959).
27. Carapito, C. et al. MSDA, a proteomics software suite for in-depth Mass Spectrometry Data Analysis using grid computing. *Proteomics* **14**, 1014–1019 (2014).
28. Bouyssié, D. et al. Proline: an efficient and user-friendly software suite for large-scale proteomics. *Bioinformatics* **36**, 3148–3155 (2020).
29. Wieczorek, S. et al. DAPAR & ProStaR: software to perform statistical analyses in quantitative discovery proteomics. *Bioinformatics* **33**, 135–136 (2017).
30. Perez-Riverol, Y. et al. The PRIDE database resources in 2022: a hub for mass spectrometry-based proteomics evidences. *Nucleic Acids Res.* **50**, D543–D552 (2022).
31. Hering, H. et al. Laser irradiation of organic tattoo pigments releases carcinogens with 3,3'-dichlorobenzidine inducing DNA strand breaks in human skin cells. *J. Invest. Dermatol.* **138**, 2687–2690 (2018).
32. Larese Filon, F., Mauro, M., Adami, G., Bovenzi, M. & Crosera, M. Nanoparticles skin absorption: new aspects for a safety profile evaluation. *Regul. Toxicol. Pharmacol.* **72**, 310–322 (2015).
33. Tompkins, L. M. & Wallace, A. D. Mechanisms of cytochrome P450 induction. *J. Biochem. Molec Toxicol.* **21**, 176–181 (2007).
34. Nebert, D. W. & Dalton, T. P. The role of cytochrome P450 enzymes in endogenous signalling pathways and environmental carcinogenesis. *Nat. Rev. Cancer*. **6**, 947–960 (2006).
35. Costa, C. et al. Exposure of human skin to benzo[a]pyrene: role of CYP1A1 and aryl hydrocarbon receptor in oxidative stress generation. *Toxicology* **271**, 83–86 (2010).
36. Esser, C., Bargen, I., Weighardt, H., Haarmann-Stemmann, T. & Krutmann, J. Functions of the aryl hydrocarbon receptor in the skin. *Semin Immunopathol.* **35**, 677–691 (2013).
37. Shiizaki, K., Kawanishi, M. & Yagi, T. Modulation of benzo[a]pyrene–DNA adduct formation by CYP1 inducer and inhibitor. *Genes Environ.* **39**, 14 (2017).
38. Binkova, B. et al. Biological activities of organic compounds adsorbed onto ambient air particles: comparison between the cities of Teplice and Prague during the summer and winter seasons 2000–2001. *Mutat. Res.* **525**, 43–59 (2003).
39. Staal, Y. C. et al. Binary PAH mixtures cause additive or antagonistic effects on gene expression but synergistic effects on DNA adduct formation. *Carcinogenesis* **28**, 2632–2640 (2007).
40. Genies, C. et al. Inhibition of the formation of benzo a pyrene adducts to DNA in A549 lung cells exposed to mixtures of polycyclic aromatic hydrocarbons. *Toxicol. Vitro*. **35**, 1–10 (2016).
41. Tarantini, A. et al. Polycyclic aromatic hydrocarbons in binary mixtures modulate the efficiency of benzo a pyrene to form DNA adducts in human cells. *Toxicology* **279**, 36–44 (2011).
42. von Koschembahr, A. et al. Metabolism and genotoxicity of polycyclic aromatic hydrocarbons in human skin explants: mixture effects and modulation by sunlight. *Arch. Toxicol.* **94**, 495–507 (2020).
43. Cui, Y., Churchwell, M. I., Couch, L. H., Doerge, D. R. & Howard, P. C. Metabolism of pigment yellow 74 by rat and human microsomal proteins. *Drug Metab. Dispos.* **33**, 1459–1465 (2005).

Acknowledgements

This work was supported by a grant from the French Agence National de la Recherche (Tattooink project, grant # ANR 21 CE34 0025). The authors wish to thank Christine Saint-Pierre from the Biomade platform (IRIG/SyMMES, CEA Grenoble, France) for her assistance in the DLS analyses. We also wish to thank Daphna Fenel for the electron microscopy analyses performed at the IBS Electron Microscope Facility (ISBG ; UAR 3518 CNRS CEA UGA EMBL) with support from the French Infrastructure for Integrated Structural Biology (FRISBI ; ANR 10 INSB 0005 02) and the GRAL Labex (CBH EUR GS (ANR 17 EURE 0003). The proteomics analyses were supported by the French Proteomic Infrastructure (ProFI; ANR-10-INBS-08-03).

Author contributions

LA and TD wrote the first draft of the manuscript. All authors reviewed the manuscript. All authors were involved in the design and/or performance of the experimental work.

Declarations

Competing interests

The authors declare no competing interests.

Supplementary Information

The online version contains supplementary material.

Additional information

Supplementary Information The online version contains supplementary material available at https://doi.org/10.1038/s41598-024-83713-9.

Correspondence and requests for materials should be addressed to T.D.

Reprints and permissions information is available at www.nature.com/reprints.

Publisher's note Springer Nature remains neutral with regard to jurisdictional claims in published maps and institutional affiliations.